Finite element modelling to predict reinforced concrete corrosion-induced cracking

José H. Castorena-González[a], Citlalli Gaona-Tiburcio[b], David M. Bastidas[c,✉], Rosa E. Núñez-Jáquez[a], José M. Bastidas[d], Facundo M. Almeraya-Calderón[b]

[a]Universidad Autónoma de Sinaloa (UAS), Facultad de Ingeniería Mochis, Gral.
Angel Flores & Fuentes de Poseidon, Jiquilpan, 81223, Los Mochis, Sinaloa, México
[b]Universidad Autónoma de Nuevo León, FIME - Centro de Innovación e Investigación en Ingeniería Aeronáutica,
Av. Universidad s/n, Ciudad Universitaria, 66455 Nuevo León, México
[c]National Center for Education and Research on Corrosion and Materials Performance, NCERCAMP-UA, Dept. Chemical,
Biomolecular, and Corrosion Engineering, The University of Akron, 302 E Buchtel Ave, Akron, OH 44325-3906, United States
[d]Centro Nacional de Investigaciones Metalúrgicas (CENIM, CSIC), Avda. Gregorio del Amo 8, 28040 Madrid, Spain

(✉Corresponding author: dbastidas@uakron.edu)

ABSTRACT: A finite element (FE) method was proposed to calculate the corrosion penetration depth (r_{crit}) on steel reinforcement necessary for the first visible crack to appear on the concrete cover. The FE analysis was carried out using the commercial software from ANSYS. The obtained FE method is a function of free concrete cover depth (C), reinforcement diameter (D), length of the anodic zone (L), and concrete type. The results show a strong influence of localized corrosion (small-size anode versus large-size cathode) on the prediction of the r_{crit} value. This influence can only be analysed three-dimensionally. The proposed FE method is validated with experimental results from literature. This approach is a novelty in considering the longitudinal direction in the analysis to account for the extension of the anodic cell. Corrosion type strongly depends on the C/L ratio, this leads to uniform corrosion for values between $0.02<C/L<0.1$ and localized corrosion for values between $0.5<C/L<4.0$.

KEYWORDS: Concrete cracking; Concrete cover depth; Corrosion penetration depth; Finite element method; Localized corrosion; Modelling; Steel reinforcements

RESUMEN: *Predicción del agrietamiento inducido por corrosión en hormigón armado mediante modelización por elementos finitos*. Este trabajo propone un método de elementos finitos (FE) para calcular la profundidad de penetración por corrosión (r_{crit}) en las armaduras de acero, necesaria para originar la aparición de la primera grieta visible en el recubrimiento de hormigón. El análisis por FE se ha llevado a cabo utilizando el programa comercial ANSYS. El método de FE obtenido se ha desarrollado en función del espesor del recubrimiento de hormigón libre (C), el diámetro de la armadura (D), la longitud de la zona anódica (L), y el tipo de hormigón. Los resultados obtenidos muestran una gran influencia de la corrosión localizada (pequeñas zonas anódicas frente a grandes zonas catódicas) en la predicción del valor de r_{crit}. Esta influencia sólo puede ser analizada tridimensionalmente. El modelo de FE propuesto se validó utilizando datos de la bibliografía. La originalidad del procedimiento propuesto radica en la consideración de la dirección longitudinal en el análisis, para tener en cuenta la extensión de la zona anódica. El tipo de corrosión tiene una gran dependencia de la relación entre C/L, ocasionando corrosión uniforme para valores entre $0,02<C/L<0,1$, y originando corrosión localizada para valores entre $0,5<C/L<4,0$.

PALABRAS CLAVES: Agrietamiento hormigón; Armaduras acero; Corrosión localizada; Espesor recubrimiento hormigón; Método elementos finitos; Modelización; Profundidad penetración corrosión

ORCID ID: José H. Castorena (https://orcid.org/0000-0001-9978-4455); Citlalli Gaona-Tiburcio (https://orcid.org/0000-0001-9072-3090); David M. Bastidas (https://orcid.org/0000-0002-8720-7500); Rosa E. Núñez-Jáquez (https://orcid.org/0000-0003-2330-6187); José M. Bastidas (https://orcid.org/0000-0001-9616-0778); Facundo M. Almeraya-Calderón (https://orcid.org/0000-0002-3014-2814)

1. INTRODUCTION

Reinforced concrete (RC) is one of the most widely used materials in the construction sector because of its versatility, cost and durability. The highly alkaline environment (pH above 12.5) of a good quality concrete leads to the formation of a passive layer on the embedded steel rebar, protecting it from corrosion and assuring a low steel corrosion rate of less than 1.16 μm/year (González *et al.,* 1996; García *et al.,* 2012; Fajardo *et al.,* 2014). However, this protective passive layer can be disrupted when the pH of the concrete pore solution is lowered, e.g. by environmentally-induced carbonation, or when aggressive chloride ions from de-icing salts, direct contact with seawater or exposure to marine aerosols reach the reinforcement or are directly added during the mixing process as an admixture, enabling diffusion to the steel surface (Jaegermann, 1990; Chung *et al.,* 2008).

Steel corrosion and the loss of rebar cross-section take place in the presence of oxygen and water through an electrochemical process (Ahmad, 2003). In general, the iron ions released from the steel react with oxygen to generate chemically stable iron oxides which are deposited on the steel surface. The spatial gap left by the consumed iron is not enough to accommodate these oxides, which have a higher volume and lower density than iron (Sánchez-Deza *et al.,* 2017), and their growth generates pressure on the surrounding concrete cover. When the expansion stress of the iron oxides surpasses that of the concrete, cracking and spalling can take place (Sánchez-Deza *et al.,* 2018).

Depending on the location of the anode and the cathode, steel reinforcement corrosion may occur in micro-cells, where anodic and cathodic half-cell reactions occur in the same place, or in macro-cells where corroded zones (anode) are distinguished from uncorroded zones (cathode) (González *et al.*, 1995; Elsener, 2002). The latter case is very important because the higher the cathode to anode surface area ratio, the faster the dissolution of the rebar cross-section, originating a high level of steel corrosion (Raupach, 1996). Most of the research works reported in the literature, in relation with the corrosion penetration depth (r_{crit}) on steel necessary to induce concrete cover cracking, they have considered uniform corrosion conditions (micro-cells), and only a few cases have assessed non-uniform corrosion (macro-cells) (Torres-Acosta and Sagüés, 2004; Busba and Sagüés, 2013). Thus it may be of interest to carry out a detailed analysis of the length of the anodic zone (*L*) defined above.

Analytical efforts have been made to propose a model that can predict either the time to corrosion-induced concrete cover cracking of a corroded structure or the residual flexural strength of RC beams subjected to rebar corrosion (Bažant, 1979; Hutchinson and Suo, 1992; Molina *et al.*, 1993; Andrade *et al.*, 1993; Liu and Weyers, 1998a; Liu and Weyers, 1998b; Martín-Pérez, 1999; Balafas and Burgoyne, 2010; Balafas and Burgoyne, 2011; Pantazopoulou and Papoulia, 2001; Vu *et al.*, 2005; Oh *et al.*, 2009; Zhang *et al.*, 2017). Such studies have used a thick-walled cylinder model to calculate the stress generated by iron oxides (Bažant, 1979), have evaluated oxide formation in partially cracked cylinders (Liu and Weyers, 1998a; Liu and Weyers, 1998b; Martín-Pérez, 1999), and have applied the FE theory (Molina *et al.*, 1993; Andrade *et al.*, 1993; Pantazopoulou and Papoulia, 2001).

The aim of this paper is to develop a numerical method by FE methodology to calculate the r_{crit} on reinforcing steel in concrete and its validation through experimental results from the literature. In this way it is proposed to analyse the parameters which define the mechanical properties of the concrete based on the stress-strain response curve as the concrete is damaged by stress.

2. EXPERIMENTAL PROCEDURE

2.1. Description of the Problem

A model is proposed to describe the problem, which consists of a steel rebar with an initial radius (r_0) embedded in concrete, the distance from the steel rebar centre to the nearest free concrete surface is defined by the R_c parameter ($R_c = C + r_0$), where C is the free concrete cover depth; and r_0 as defined above, R_c, C, and r_0 are showed in Fig. 1. In order to model the concrete cover cracking, the expansion strength of the iron oxide layer (δ) was included (see Fig. 1), i.e. the iron oxide layer required to generate a similar tangential stress (σ_t) to the maximum tensile strength of the concrete (f_t) to start the cracking process at the steel/concrete interface (Bhargava *et al.*, 2005).

The reliability of the common thick-walled concrete cylinder approach, under the action of internal pressure originated by the expansion of iron oxide of the corroded steel rebar, is only approximate (Sánchez-Deza *et al.*, 2018). This may be attributed to the boundary conditions, see Fig. 1, around the corroded steel rebar, because the residual resistance of the cracked concrete cover is ignored (Pantazopoulou and Papoulia, 2001). To avoid these problems, corroded steel rebar is described as a structural element which is forced to occupy the volume inside a hollow-core concrete cylinder whose interior diameter (*D*), $D = 2r_0$, is smaller than the diameter of the corroded steel rebar, $2r_0 + \delta$. When both steel and concrete are coupled it is possible to calculate the pressure generated between them.
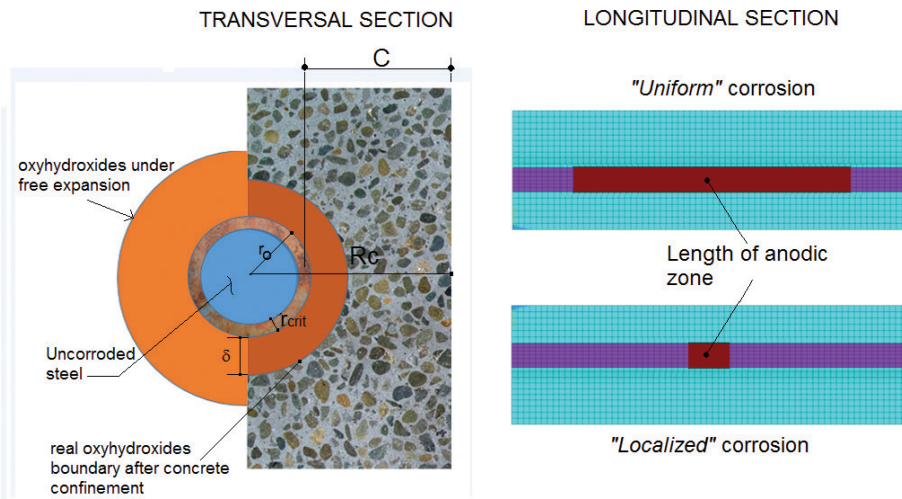
FIGURE 1.   Model's parameters for the estimation of stresses during corrosion process. C is the free concrete cover depth, R_c is the distance from steel rebar to the nearest free concrete surface, r_0 is the initial radius of steel rebar, and δ is the iron oxides layer.

2.2. FE Method for the Steel/Oxide/Concrete System

In order to describe the steel/concrete interface, contact elements may be used, which are considered as layers without thickness that adhere to the surfaces and allow them to come into contact. One side of the contact element is referred to as the '*contact surface*' and the other side as the '*target surface*'. The contact surface is a highly non-linear feature. In the present analysis, the contact surface adheres to the steel rebar, while the target surface adheres to the surrounding concrete, since it is assumed that the rust pushes on the concrete. To use contact elements, it is necessary to define their stiffness properties. If stiffness is very high, fluctuation and convergence problems may occur in the numerical calculation process, limiting the magnitude of δ.

When using contact elements, the main difficulty is that the contact surface between the two bodies is unknown in advance. Under ideal conditions, an initial value of δ is obtained by solving the problem through the elasticity theory for a homogeneous material (Timohenko and Goodier, 1970):

$$\delta = 2r_0 P_g \left[\frac{1-v_s}{E_s} + \frac{(1+v_c)R_c^2 + (1-v_c)r_0^2}{E_c \left(R_c^2 - r_0^2 \right)} \right] \quad (1)$$

where P_g is the radial pressure at the steel/concrete interface; v_s is the Poisson's coefficient of steel; E_s is the modulus of elasticity for reinforcement steel; v_c is the Poisson's coefficient of concrete; E_c is the modulus of elasticity for concrete; r_0 and R_c have been defined above. It is possible to demonstrate that

P_g parameter can be calculated using the expression (Wang, 1953):

$$f_t = \left(\frac{R_c^2 + r_0^2}{R_c^2 - r_0^2} + v_c \right) P_g \quad (2)$$

where all parameters have been defined previously.

In order to calculate δ and P_g parameters using Eq. (1) and Eq. (2), respectively, it is assumed that the concrete is not cracked and the elasticity theory for a homogeneous material may be utilized. When the iron oxide layer grows and reaches the value of δ, the concrete starts to crack at the corroded steel/concrete interface. For values higher than δ it is not possible to use the elasticity theory, although the concrete cover still maintains some residual tensile strength. This process is modelled by FE method as follows.

A 3D model for the FE method has been utilized to represent the interaction of the steel/oxide/concrete system, on which the compressibility of rust products is not considered, and the expansion of corrosion products, denoted by δ, is uniformly distributed around the reinforcing steel. (i) The concrete has been modelled using the three-dimensional element SOLID65 (from ANSYS) defined by 8 nodes and 3 degrees of freedom in each node: displacements in the x, y and z axes. This software has the capacity to represent concrete failure due to tension and compression by means of cracks which occur at the integration points along the three orthogonal directions, once the concrete's resistance to stress and compression has been reached. Figure 2 shows the stress-strain curve for concrete using theoretical compressive strength values (f_c') (Thorenfeldt *et al.*, 1987; Popovics, 1973). In Fig. 2

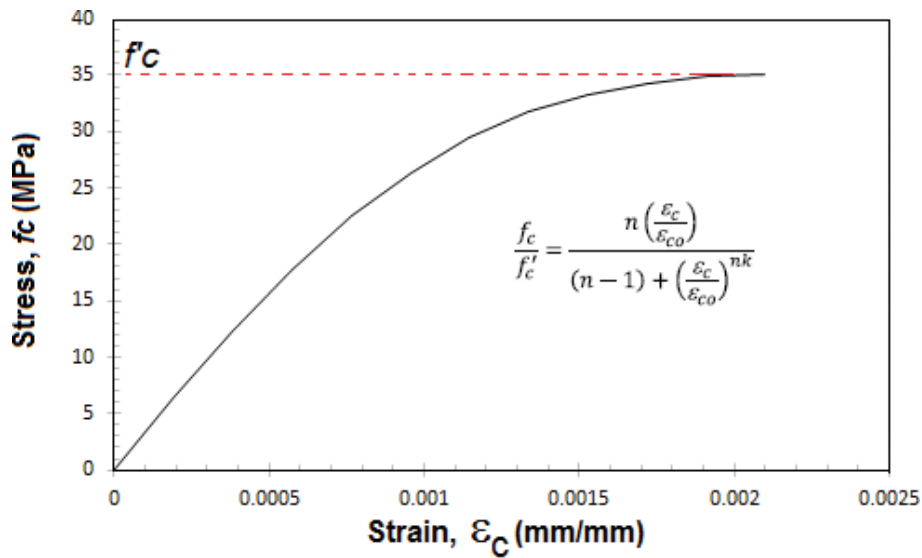FIGURE 2.   Stress-strain curve for concrete. Considering $n=2$, $\varepsilon_0=0.0021$, $f_c' =35$ MPa, and $k=1$. Where n and k are mechanical properties parameters, ε_0 is the unit strain in concrete at the compressive strength of concrete (f_c').
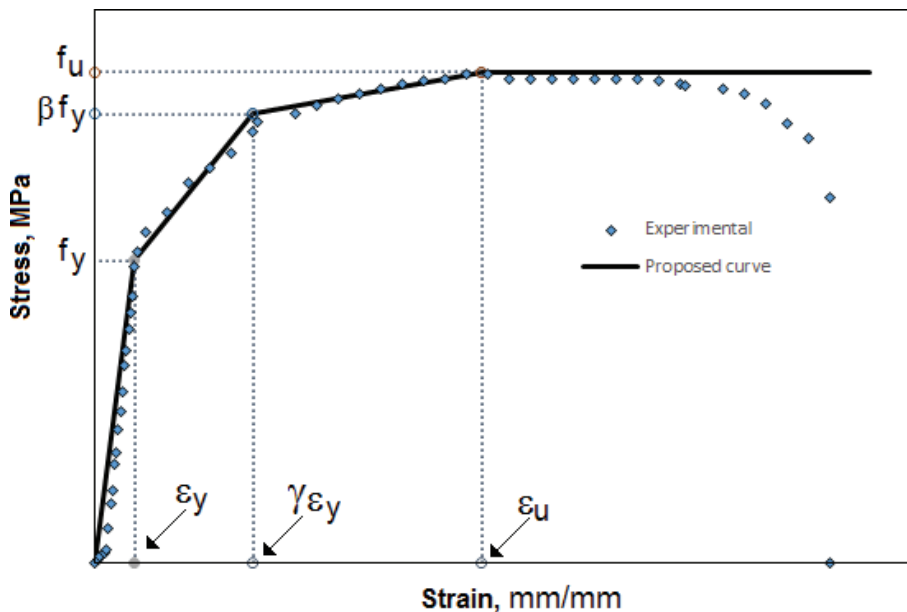

FIGURE 3.   Tri-linear stress-strain curve for steel. Where ε_u is the unit strain in reinforcing steel at the f_u ultimate strength, and ε_y is the unit strain in reinforcing steel at the f_y yield strength.

the compressive strength of 35 MPa and strain of 0.002 are used for illustration, these values are variable parameters in the proposed model, while n and k are constant, with values of 2 and 1, respectively. The tensile stress-strain relation adopted for concrete is the cracking criterion achieving the concrete tensile strength. (ii) The reinforcing steel properties can be modelled using the plasticity model, which considers the strain hardening effect. Figure 3 shows

the tri-linear proposed stress-strain curve that may be adjusted to experimental data as a function of the yield strength (f_y) and the ultimate strength (f_u). And finally, (iii) the use of contact elements for friction modelling associated to iron oxide layers often involves great converge problems in the fitting process due to their highly non-linear behaviour. Friction and stiffness (also called 'penalty stiffness') are dependent upon the type of iron oxide layer and

the permissible penetration is obtained from the FE method analysis. The most important challenge in modelling with contact elements is to determine when the two surfaces come into contact, and this depends on several factors such as the separation between them or the mesh size used.

It is assumed that the reinforcing steel and the surrounding concrete cover always remain in contact, but with the possibility of sliding, it is necessary to provide a friction coefficient, contact stiffness, and permissible penetration parameters. Steel r_{crit} (see Fig. 1) may be calculated using the expression (Castorena, 2007):

$$r_{crit}^2 - 2r_0 r_{crit} + \frac{(R_c + r_0)\delta}{(\alpha - 1)} = 0 \qquad (3)$$

where α is the molar volume ratio coefficient; and the other parameters have been defined previously. The molar volume (V_m, cm^3·mol^{-1}) of an iron oxide is defined as the ratio between the molar mass and the density of a given oxide phase. Table 1 presents the α coefficient of oxide molar volume expansion to iron consumed in the corrosion process for a marine environment in the presence of chloride ions (Sánchez-Deza et al., 2017; Sánchez-Deza et al., 2018):

$$a = V_{m(oxide)} / V_{m(Fe)} \qquad (4)$$

where $V_{m(oxide)}$ and $V_{m(Fe)}$ are the molar volumes of oxide and iron, respectively. The α coefficient indicates the increase in volume during the corrosion process (Sánchez-Deza et al., 2017). The high α coefficient of akaganeite (3.29) may accelerate the cracking process more than the other five oxide phases: lepidocrocite (3.16), goethite (2.94), maghemite (2.30), hematite (2.13), and magnetite (2.09).

TABLE 1. Molar volume (V_m) and molar volume expansion ratio coefficient (α) ($\alpha = V_{m(oxide)}/V_{m(Fe)}$) for oxides of iron generated in a marine environment (Sánchez-Deza et al., 2017; Sánchez-Deza et al., 2018).

Iron and Iron Oxide Phase	Molar Volume (V_m), (cm^3·mol^{-1})	Molar Volume Expansion Ratio Coefficient (α)
Iron, Fe	7.09	–
Akaganeite, β-FeOOH	23.32	3.29
Goethite, α-FeOOH	20.82	2.94
Lepidocrocite, γ-FeOOH	22.42	3.16
Hematite, α-Fe$_2$O$_3$	30.27	2.13
Maghemite, γ-Fe$_2$O$_3$	32.63	2.30
Magnetite, Fe$_3$O$_4$	44.52	2.09

The smeared crack model proposed by Pantazopoulou and Papoulia (2001) was used to calculate the width of the crack (w) using results yielded by the FE method, i.e. the average deformation around the fictitious perimeter generated by the R_c is obtained using the formula:

$$w = 2\pi R_c \varepsilon_t \qquad (5)$$

where ε_t is the strain in polar coordinates; and R_c has been defined above.

The procedure to carry out the non-linear FE method analysis is as follows, the mechanical properties of the concrete are defined by: (a) their stress-strain curves, (b) the steel diameter ($D=2r_0$), (c) the C, and (d) the L parameters. With these four parameters a first δ value is obtained using Eq. (1) which may simulate the oxide thickness (δ) necessary for corrosion cracking to start. With this δ value, the three parameters required in the contact elements are: (1) friction, (2) stiffness, and (3) permissible penetration. These input parameters together with the number of FEs were adjusted. For example, if the corrosion products are mainly of lepidocrocite type, then a coefficient of friction of 0.458, a normal contact stiffness of 4000 (force/length), and a permissible penetration factor of 0.1 are used as properties of the contact element. Once the parameters for the contact elements have been established, the δ value is then increased, accompanied by α value according to the type of iron oxide (see Table 1), until the crack reaches the surface of the concrete cover. This is defined as the first visible crack. At this point, Eq. (3) is applied to calculate r_{crit}, and Eq. (5) is applied to yield the width (w) of this first visible crack. The analysis allows the value of δ to be raised even further, so that a relationship between r_{crit} and w can be obtained beyond the first time a visible crack appears.

The strategy followed in the present analysis to avoid convergence problems is similar to the proposal by Mohyeddin et al. (2013), i.e. to apply a δ value in several large steps, and when the program fails due to convergence problems to note the corresponding step number and then repeat the analysis with smaller steps until convergence failure occurs again, noting the step in which this happens, and so on.

3. EXPERIMENTAL RESULTS AND DISCUSSION

3.1. Validation of the FE Method

To validate the present FE method results from Torres-Acosta and Sagües (2004) were used, in which 14 cylindrical concrete specimens were analysed. Each reinforcement has a pipe tubular part

composed of three regions: two end regions protected with PVC covers and an exposed central region (anodic zone) to measure deformation and to calculate the pressure during an accelerated corrosion process applying a current density of 0.1 mA·cm^{-2}.

Figure 4 shows the output results for a cylindrical cross-section and a rectangular cross-section (denominated beam). For this first step of the validation, i.e. when the first crack appears at the steel/concrete interface, it was assumed that the value of L has no influence, because identical results were obtained for different L values. It should be noted that the importance of Fig. 4 results is because they are utilized to calculate r_{crit} by FE method modelling of a reinforcement with a cylindrical shape, due to their symmetry and simplification of the calculation,

and that it is equally applicable for beams of rectangular section.

During the second step, when the first visible crack appears on the concrete cover surface, the numerical FE method and the experimental results from Torres-Acosta and Sagüés (2004) are shown in Fig. 5 as an example. This figure shows details of the state of cracking and pressure in the contact elements at the most important points of the curve, i.e. the first crack at the steel/concrete interface, the maximum pressure, and the first visible crack. The part where the first crack appears at the steel/concrete interface is coincident because at this point, the FE method always matches with the experimental results. Figure 6 shows tangential stress (σ_t) on concrete due to localized corrosion of an anodic zone having a length L, where L determines the length
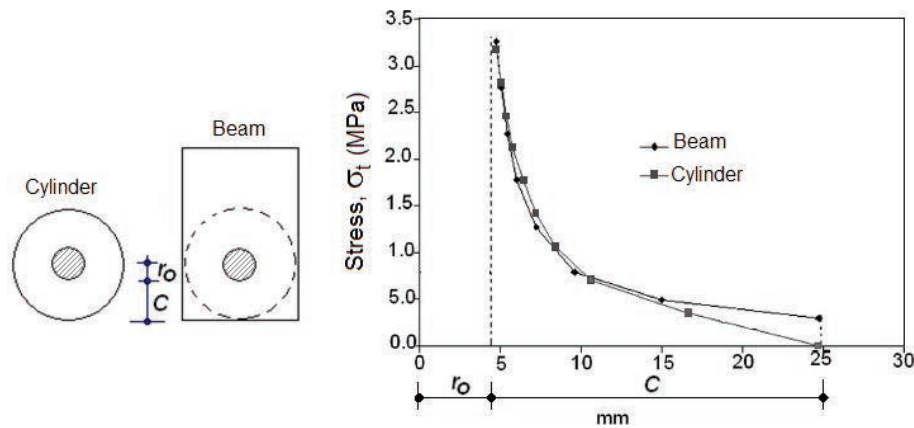

FIGURE 4. Comparison between tangential stress (σ_t, MPa) results obtained for different boundary conditions (cylinder and beam). r_0 is the radius of the steel reinforcement (mm), and C is the free concrete cover depth. Parameters used in the simulation: free concrete cover depth (C=20 mm), modulus of elasticity of concrete (E_c=28836 MPa), Poisson's coefficient of concrete (v_c=0.24), steel reinforcement radius (r_0=4.75 mm), modulus of elasticity of reinforcing steel (E_s=210000 MPa), and Poisson's coefficient of reinforcing steel (v_s=0.3).
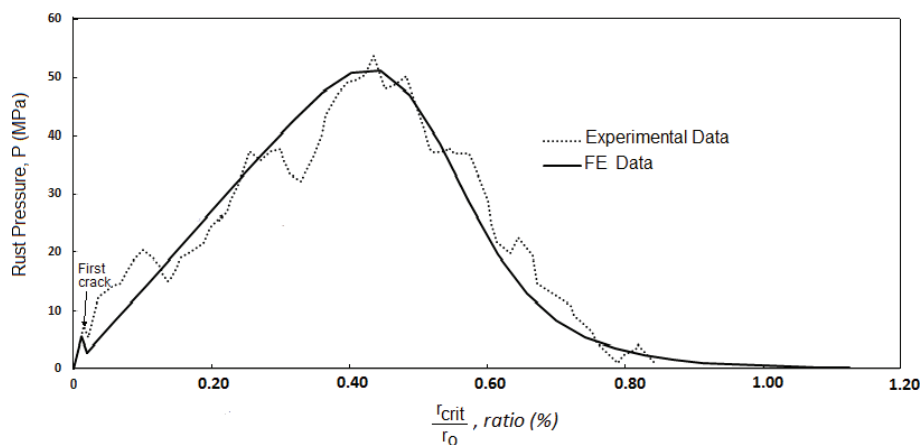

FIGURE 5. Variation of pressure (P_c) originated by expansion of iron oxides and the ratio of corrosion penetration depth on steel and initial radius of steel rebar (r_{crit}/r_0) at the steel/concrete interface. "First Crack" indicates that cracking of concrete initiates at the steel/concrete interface.
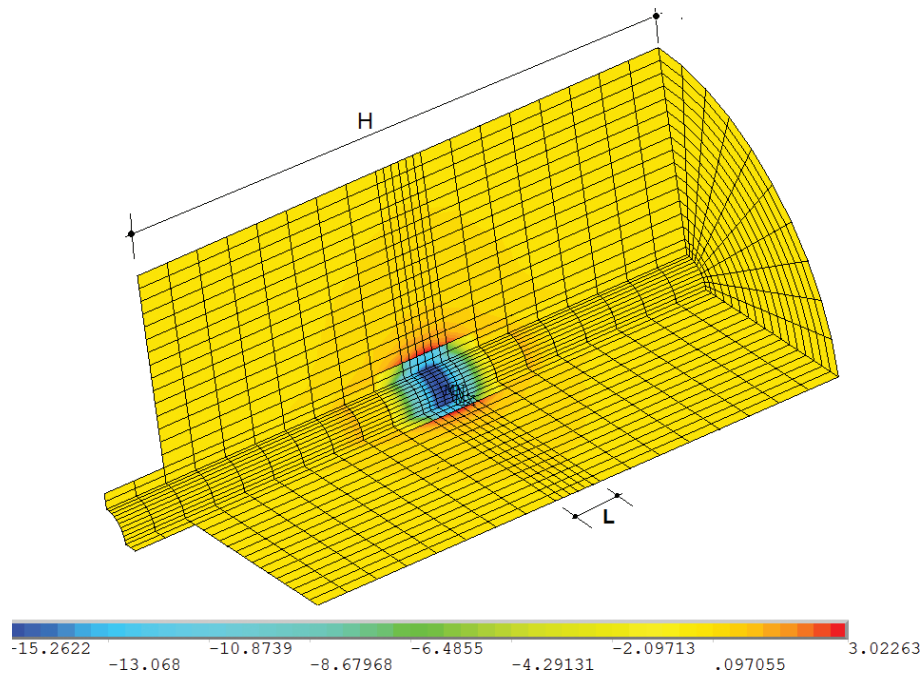
FIGURE 6. Tangential stresses (σ_t) in concrete due to localized corrosion. Parameters used in the simulation: D=102 mm, H=406 mm, L=92 mm, C/D=0.9, C/L=0.4, and Poisson's coefficient of concrete ν_c=0.24.

along which parameter δ is imposed at the steel/concrete interface. For simplicity, one quarter part of the cylinder was considered to be representative. After a converge analysis, it is sufficient to use 4020 finite elements, that is 3300 to simulate the concrete (SOLID65), 480 to simulate the steel (SOLID45), and 240 to simulate the contact elements.

For a given ratio of C/D, and taking into account the properties of the concrete (compressive strength, tensile strength, and modulus of elasticity), the model is validated according to the calculated values of δ and P_g using Eq. (1) and Eq. (2), respectively. Later, using different C/D ratios, a total of 100 different cases have been analysed using the FE method and a regression analysis method using the statistical analysis system (SAS) program, with a correlation coefficient R^2=0.9200. The obtained model is described by the proposed expression:

$$r_{crit} = 5.272 \times 10^{-3} \left(\frac{C}{D} \right)^{0.267} \delta^{-0.435} \left(\frac{C}{L} \right)^{0.467} \quad (6)$$

where C/D and C/L have been defined previously and δ is calculated using Eq. (1). The influence of concrete properties is implicit in the calculation of δ, see Eq. (1). The applicability of the present model, described by Eq. (6), is shown in Fig. 7. A good fit can be observed comparing results obtained using Eq. (6) and experimental results from Torres-Acosta and Sagüés (2004). It should be noted that Eq. (6) has been used for experimental results other

than those used for the comparing of the model (Castorena et al., 2008), and the use of Eq. (6) is applicable to situations where the concrete might be confined by compressive stress fields or stirrups/ties.

3.2. Influence of Type and Size of Specimens on r_{crit}

The influence of mechanical properties of concrete and geometrical conditions of steel rebar on r_{crit} defined by Eq. (6) was analysed. The influence of compressive strength of concrete was evaluated using a range of f_c' values between 20 MPa and 70 MPa. Where f_c' value is implicitly included in Eq. (6), given that for the calculation of δ it is necessary to use Eq. (1). The other mechanical properties values are function of f_c', that is, modulus of elasticity (E_c) and tensile strength (f_t) (Mohyeddin et al., 2013; ACI 318M−08, 2008). To analyse the influence of these variables, C/D values were chosen between 0.5 and 8.0. Two extreme C/L values were used: C/L=0.05 (Fig. 8) for uniform corrosion, and C/L=2.5 (Fig. 9) for localized corrosion. As it is observed in Figs. 8 and 9, the influence of concrete properties in the estimation of r_{crit} is not relevant, possibly because of the difference in stiffness between steel and concrete, which is on the order of 7 to 8 times as average. This fact is of great practical importance, since Eq. (6) can be used in existing reinforced concrete structures, in which the values of the properties of the concrete used in its construction are not known with precision.
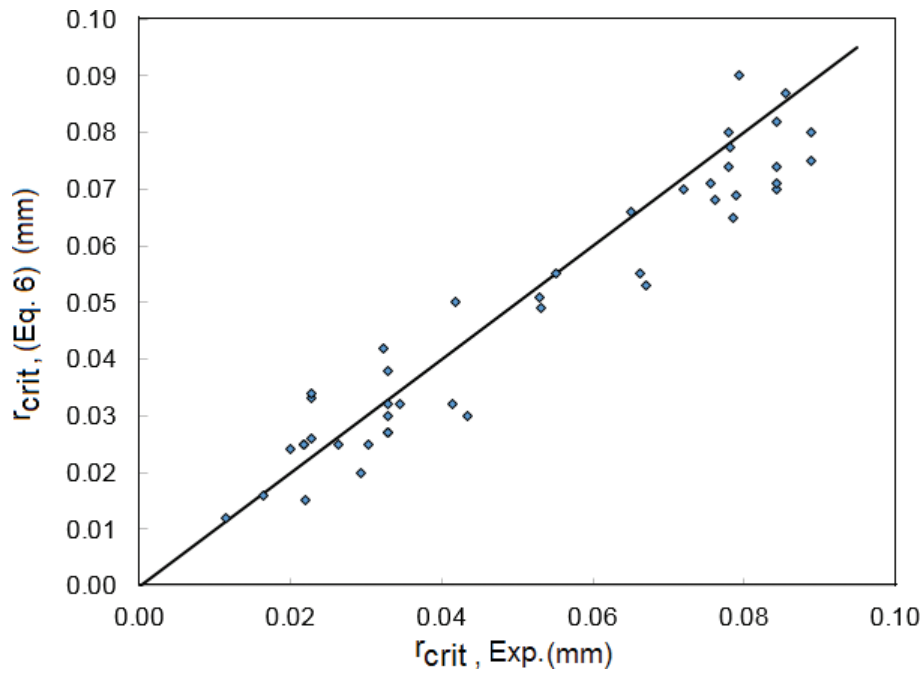
FIGURE 7. Comparison between results obtained using the present FE method (r_{crit} using Eq. (6)), and experimental results (r_{crit} Experimental) obtained from Torres-Acosta and Sagüés (2004).
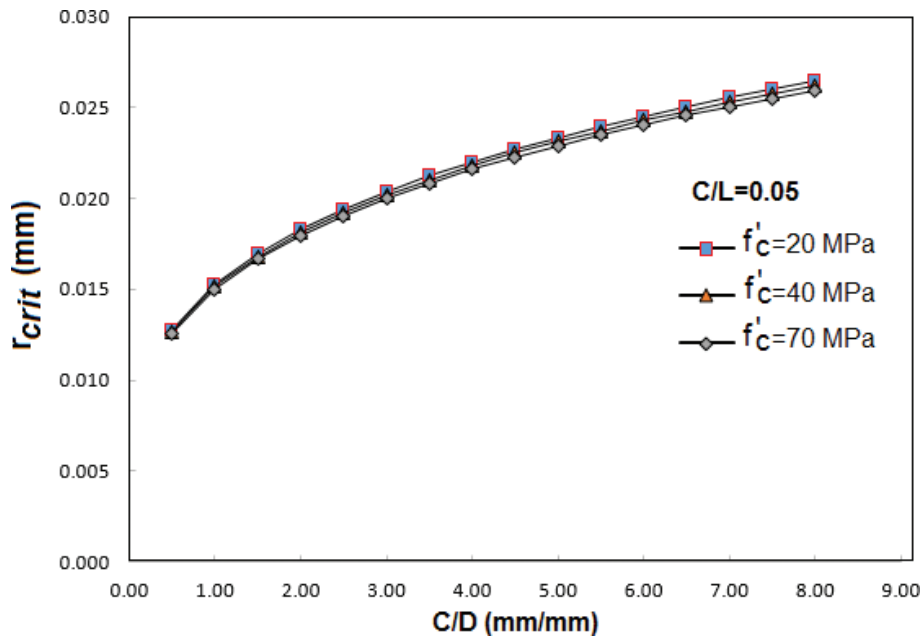

FIGURE 8. Influence of the mechanical properties of concrete on r_{crit} for a *C/L* ratio of 0.05.

Figure 10 shows the influence of steel reinforcement diameter (*D*=9.5, 19 and 38 mm) on r_{crit} for a f_c value of 35 MPa and a *C/L* ratio of 1.0. Implicitly, the value of the rebar diameter is related to the δ variable, see Eq. (1). Contrary to the influence of concrete properties (Figs. 8 and 9) the influence of the δ parameter is important (see Fig. 10). This behaviour is derived from the geometric conditions between the diameter of the steel reinforcement (*D*) and the free concrete cover depth (*C*), as r_0 appears to be as power of two in Eq. (1).
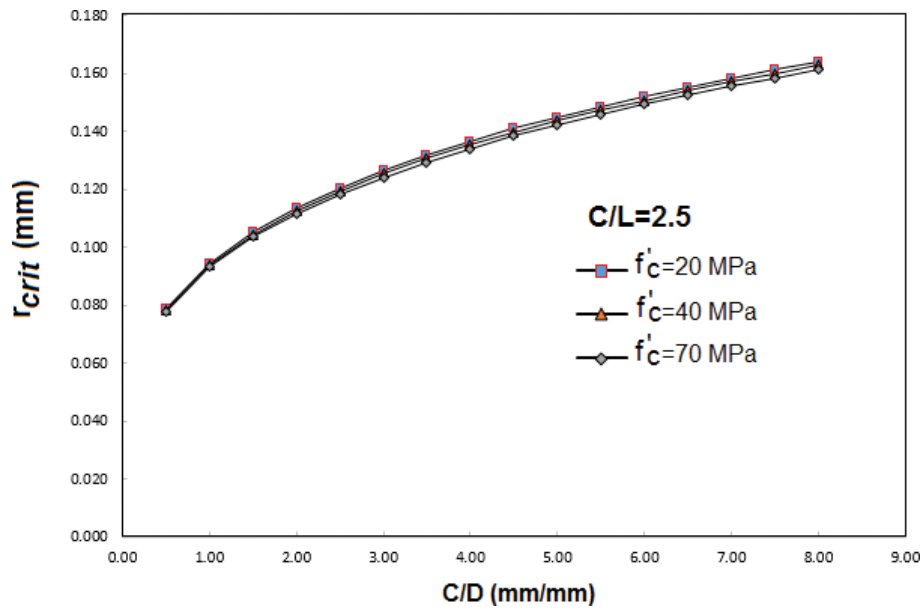
FIGURE 9.   Influence of the mechanical properties of concrete on r_{crit} for a C/L ratio of 2.5.
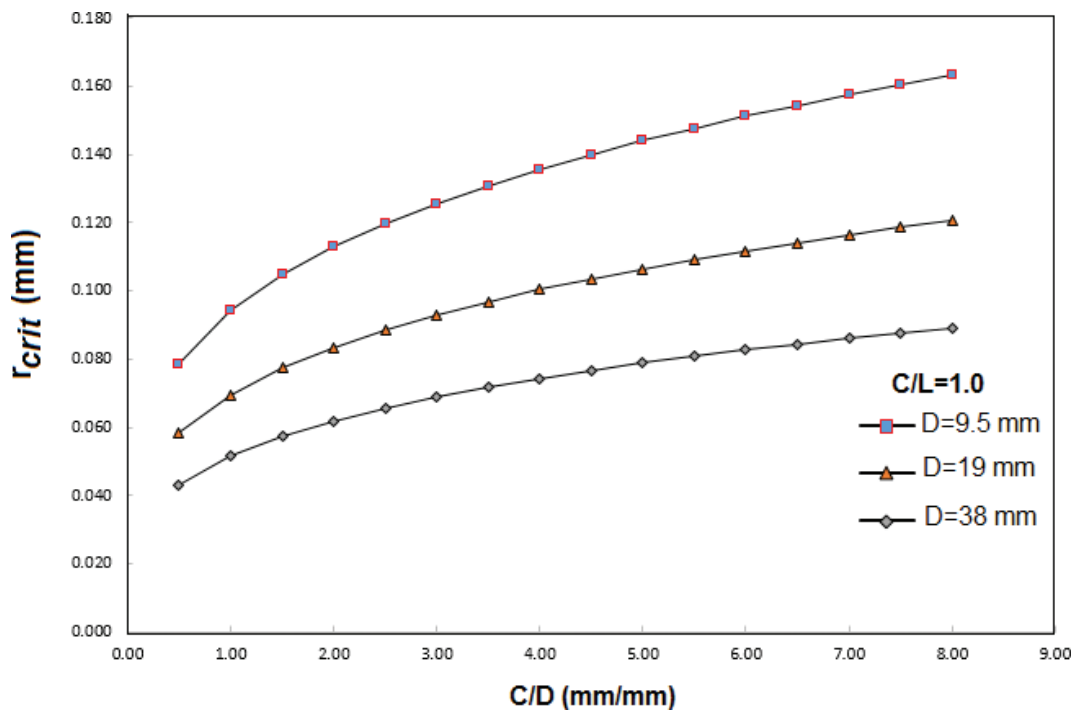

FIGURE 10.   Influence of the size of the steel reinforcement diameter, D=9.5, 19 and 38 mm on r_{crit} for f'_c =35 MPa, and C/L=1.0.

Finally the influence of C/L ratio on r_{crit} was analysed, taking f'_c and δ values as 35 MPa and 0.002632 mm, respectively. The C/L values were over the range of 0.02 (uniform corrosion) and 4.0 (localized corrosion). After the numerical analysis the results obtained were plotted in Fig. 11, in which the importance of C/L ratio on the value of r_{crit} is shown. From the analysis of Fig. 11, it can be concluded that for relations comprised $0.02<C/L<0.10$, the reinforced concrete element undergoes uniform corrosion (that is, there is little influence of the C/L ratio on r_{crit}), and for values between the range $0.5<C/L<4.0$, the reinforcement suffers localized corrosion.
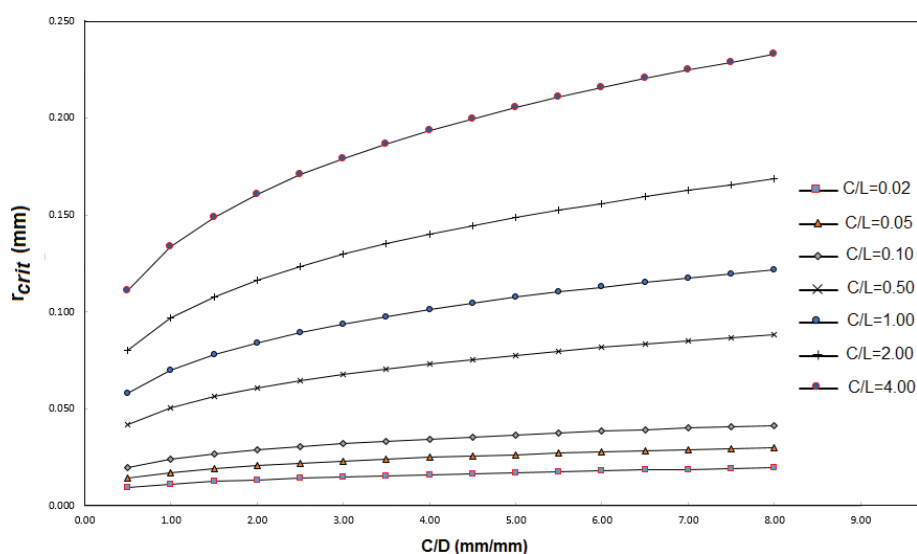
FIGURE 11.   Influence of *C/D* parameter on r_{crit} for different *C/L* ratios: *C/L*=0.02, 0.05, 0.1, 0.5, 1.0, 2.0 and 4.0.

4. CONCLUSIONS

Based on the results of this experimental investigation under marine environment, the following conclusions are drawn:

- Using contact elements methodology it is possible to model initiation and propagation stages of the concrete cover cracking due to corrosion of steel reinforcements.
- A FE method is proposed to determine the corrugated steel corrosion penetration depth at the point when the first visible crack appears. The FE method is based on geometry, free concrete cover depth (*C*), steel reinforcement rebar diameter (*D*), anodic zone length (*L*), and the mechanical properties of the concrete: modulus of elasticity, compressive strength, Poisson's modulus, and tensile strength.
- A good correlation was found between experimental results from the literature and the developed FE method. Corrosion type (uniform or localized) strongly depends on the *C/L* ratio. For a *C/L* ratio value comprised 0.02<*C/L*<0.10 the steel reinforcement presents uniform corrosion, while for higher a *C/L* ratio value of 0.5<*C/L*<4.0 the reinforcement suffers localized corrosion.

ACKNOWLEDGEMENTS

REFERENCES

ACI 318M−08 (2008). Building Code Requirements for Structural Concrete and Commentary, American Concrete Institute, Farmington Hill, Michigan.

Ahmad, A. (2003). Reinforcement corrosion in concrete structures, its monitoring and service life prediction–A review. *Cement. Concrete Comp.* 25 (4−5), 459−471. https://doi.org/10.1016/S0958-9465(02)00086-0.

Andrade, C., Alonso, C., Molina, F.J. (1993). Cover cracking as a function of bar corrosion; Part I-Experimental test. *Mater. Struct.* 26 (8), 453−464. https://doi.org/10.1007/BF02472805.

Balafas, I., Burgoyne, C.J. (2010). Environmental effects on cover cracking due to corrosion. *Cement. Concrete Res.* 40 (9), 1429−1440. https://doi.org/10.1016/j.cemconres.2010.05.003.

Balafas, I., Burgoyne, C.J. (2011). Modelling the structural effects of rust in concrete cover. *J. Eng. Mech.* 137 (3), 175−185. https://doi.org/10.1061/(ASCE)EM.1943-7889.0000215.

Bažant, Z.P. (1979). Physical model for steel corrosion in concrete sea structures application. *J. Struct. Div.-ASCE* 105 (6), 1155–1166.

Bhargava, K., Ghosh, A.K., Mori, Y., Ramanujam, S. (2005). Modelling of time to corrosion-induced cover cracking in reinforced concrete structures. *Cement. Concrete Res.* 35 (1), 2203−2218. https://doi.org/10.1016/j.cemconres.2005.06.007.

Busba, E., Sagüés, A.A. (2013). Critical localized corrosion penetration of steel reinforcement for concrete cover cracking. *NACE, Corrosion 2013 Conference*, Paper No. 2747. http://www.eng.usf.edu/~sagues/Documents/Nace%2013%202747%20Critical%20Local%20Corr%20Penetr%20Crack.pdf.

Castorena, J.H. (2007). Modelación con Elemento Finito del Daño por Corrosión en Estructuras de Hormigón Reforzado, PhD Thesis, Centro de Investigación en Materiales Avanzados (CIMAV), Universidad Autónoma de Nuevo León, Nuevo León, México.

Castorena, J.H., Almeraya-Calderón, F., Velásquez, J.L., Gaona-Tiburcio, C., Cárdenas, A.I.; Barrios-Durstewitz, C., López-León, L., Martínez-Villafañe, A. (2008). Modeling the time-to-corrosion cracking of reinforced concrete structures by finite element. *Corrosion* 64 (7), 600−606. https://doi.org/10.5006/1.3278495.

Chung, L., Najm, H., Balaguru, P. (2008). Flexural behavior of concrete slabs with corroded bars. *Cement. Concrete Comp.* 30 (3), 184−193. https://doi.org/10.1016/j.cemconcomp.2007.08.005.

Elsener, B. (2002). Macrocell corrosion of steel in concrete-implications for corrosion monitoring. *Cement. Concrete Comp.* 24 (1), 65−72. https://doi.org/10.1016/S0958-9465(01)00027-0.

Fajardo, S., Sánchez-Deza, A., Criado, M., La Iglesia, A., Bastidas, J.M. (2014). Corrosion of steel embedded in fly ash mortar using a transmission line model. *J. Electrochem. Soc.* 161 (8), E3158−E3164. https://doi.org/10.1149/2.019408jes.

García, J., Almeraya, F., Barrios, C., Gaona, C., Núñez, R., López, I., Rodríguez, M., Martínez-Villafañe, A., Bastidas, J.M. (2012). Effect of cathodic protection on steel-concrete bond strength using ion migration measurements. *Cement. Concrete Comp.* 34 (2), 242−247. https://doi.org/10.1016/j.cemconcomp.2011.09.014.

González, J.A., Benito, M., Feliu, S., Rodríguez, P., Andrade, C. (1995). Suitability of assessment methods for identifying active and passive zones in reinforced concrete. *Corrosion* 51 (2), 145−152. https://doi.org/10.5006/1.3293586.

González, J.A., Ramírez, E., Bautista, A., Feliu, S. (1996). The behavior of pre-rusted steel in concrete. *Cement. Concrete Res.* 26 (3), 501−511. https://doi.org/10.1016/S0008-8846(96)85037-X.

Hutchinson, J.W., Suo, Z. (1992). *Mixed mode cracking in layered materials*. In *Advances in Applied Mechanics*, Vol. 29, Hutchinson, J.W., Wu, T.Y. (Eds.), Academic Press, San Diego, CA, pp. 63–91.

Jaegermann, C. (1990). Effect of water-cement ratio and curing on chloride penetration into concrete exposed to Mediterranean-sea climate. *ACI Mater. J.* 87 (4) 333−339. https://doi.org/10.14359/2039.

Liu, Y., Weyers, R.E. (1998a). Modeling the time-to-corrosion cracking in chloride contaminated reinforced concrete structures. *ACI Mater. J.* 95 (6), 675−681. https://doi.org/10.14359/410.

Liu, T., Weyers, R.W. (1998b). Modeling the dynamic corrosion process in chloride contaminated concrete structures. *Cement. Concrete Res.* 28 (3), 365–379. https://doi.org/10.1016/S0008-8846(98)00259-2.

Martín-Pérez, B. (1999). Service life modelling of RC highway structures exposed to chlorides. PhD Dissertation, University of Toronto, Toronto.

Mohyeddin, A., Goldsworthy, H.M., Gad, E.F. (2013). FE modelling of RC frames with masonry infill panels under in-plane and out-of-plane loading. *Eng. Struct.* 51, 73−87. https://doi.org/10.1016/j.engstruct.2013.01.012.

Molina, F.J., Alonso, C., Andrade, C. (1993). Cover cracking as a function of rebar corrosion. Part 2-Numerical model. *Mater. Struct.* 26 (9), 532−548. https://doi.org/10.1007/BF02472864.

Oh, B.H., Kim, K.H., Jang, B.S. (2009). Critical corrosion amount to cause cracking of reinforced concrete structures. *ACI Mater. J.* 106 (4), 333–339. https://doi.org/10.14359/56653.

Pantazopoulou, S.J., Papoulia, K.D. (2001). Modelling cover-cracking due to reinforcement corrosion in RC structures. *J. Eng. Mech.* 127 (4), 342−351. https://doi.org/10.1061/(ASCE)0733-9399(2001)127:4(342).

Popovics, S. (1973). A numerical approach to the complete stress-strain curve of concrete. *Cement. Concrete Res.* 3 (5), 583−599. https://doi.org/10.1016/0008-8846(73)90096-3.

Raupach, M. (1996). Chloride-induced macrocell corrosion of steel in concrete–theoretical background and practical consequences. *Constr. Build. Mater.* 10 (5), 329−338. https://doi.org/10.1016/0950-0618(95)00018-6.

Sánchez-Deza, A., Bastidas, D.M., La Iglesia, A., Bastidas, J.M. (2017). A simple thermodynamic model on the cracking of concrete due to rust formed after casting. *Anti-Corros. Method. Mater.* 64 (3), 335−339. https://doi.org/10.1108/ACMM-11-2015-1602.

Sánchez-Deza, A., Bastidas, D.M., La Iglesia, A., Mora, E.M., Bastidas, J.M. (2018). Service life prediction for 50-year-old buildings in marine environments. *Rev. Metal.* 54 (1), e111. https://doi.org/10.3989/revmetalm.111.

Thorenfeldt, E., Tomaszewicz, A., Jensen, J.J. (1987). Mechanical properties of high-strength concrete and applications in design. *Proc. Symposium on Utilization of High-Strength Concrete,* Tapir, Trondheim, Norway, pp. 149−159.

Timoshenko, S., Goodier, J. (1970). *Theory of Elasticity*. McGraw-Hill International Book Company, New York, pp. 41−46.

Torres-Acosta, A., Sagüés, A. (2004). Concrete cracking by localized steel corrosion – geometric effects. *ACI Mater. J.* 101 (6), 501−507. https://doi.org/10.14359/13489.

Vu, K., Stewart, M.G., Mullard, J. (2005). Corrosion-induced cracking: experimental data and predictive models. *ACI Struct. J.* 102 (5), 719–726. https://doi.org/10.14359/14667.

Wang, C.T. (1953). *Applied Elasticity*. McGraw-Hill International Book Company, New York.

Zhang, J., Ling, X., Guan, Z. (2017). Finite element modeling of concrete cover crack propagation due to non-uniform corrosion of reinforcement. *Constr. Build. Mater.* 132 (2), 487–499. https://doi.org/10.1016/j.conbuildmat.2016.12.019.